



Synthesis and electrical properties of scheelite $\text{Ca}_{1-x}\text{Sm}_x\text{MoO}_{4+\delta}$ solid electrolyte ceramics

Jihai Cheng^{a,b,*}, Chenfei Liu^a, Wenbing Cao^a, Mingxing Qi^a, Guoquan Shao^a

^a Department of Chemistry and Materials Engineering, Hefei University, Hefei 230022, China

^b Key Lab of Powder and Energy Sources Materials, Hefei University, Hefei 230022, China

ARTICLE INFO

Article history:

Received 9 February 2010

Received in revised form 11 November 2010

Accepted 12 November 2010

Available online 21 November 2010

Keywords:

A. Ceramics

B. Chemical synthesis

C. Impedance spectroscopy

D. Electrical properties

ABSTRACT

Scheelite-type $\text{Ca}_{1-x}\text{Sm}_x\text{MoO}_{4+\delta}$ electrolyte powders were prepared by the sol–gel auto-combustion process. The crystal structure of the samples was determined by employing the techniques of X-ray diffraction (XRD). According to the XRD analysis, the formed continuous series of $\text{Ca}_{1-x}\text{Sm}_x\text{MoO}_{4+\delta}$ ($0 \leq x \leq 0.3$) solid solutions had the structure of tetragonal scheelite, and the lattice parameters increased with increasing x in the Sm-substituted system. Results of sinterability and electrochemical testing revealed that the performances of Sm-doped calcium molybdate were superior to that of pure CaMoO_4 . $\text{Ca}_{1-x}\text{Sm}_x\text{MoO}_{4+\delta}$ ceramics show higher sinterability, and the $\text{Ca}_{0.8}\text{Sm}_{0.2}\text{MoO}_{4+\delta}$ sample with 98.7% of the theoretical density were obtained after being sintered at 1250 °C for 4 h. The conductivity increased with increasing samarium content, and a total conductivity $9.54 \times 10^{-3} \text{ S cm}^{-1}$ at 800 °C could be obtained in $\text{Ca}_{0.8}\text{Sm}_{0.2}\text{MoO}_{4+\delta}$ sintered at 1250 °C for 4 h.

© 2010 Elsevier Ltd. All rights reserved.

1. Introduction

Solid oxide fuel cells (SOFCs) have attracted increasing interest for their high energy conversion efficiency, fuel flexibility and low pollution to environment [1–3], and they exhibit relative higher specific energy among battery systems [4]. Traditional electrolyte based on yttria-stabilized zirconia (YSZ) is one of the most well known electrolyte materials for SOFCs. However, the high operating temperature (above 1000 °C) results in both high costs and system degradation at the interface between cell components [5,6]. Therefore, research and development of electrolyte materials operating at intermediate temperature have received much attention previously. Now the electrolyte materials to substitute the YSZ electrolyte materials have attracted considerable attention throughout the world.

Doped ABO_4 ($A = \text{Pb, Sr, Ca}$; $B = \text{Mo, W}$) scheelite-type materials have been studied in recent years, these scheelite-type oxides exhibit a high oxide ion conduction in intermediate temperature range, e.g., $\text{Pb}_{0.9}\text{Sm}_{0.1}\text{WO}_{4+\delta}$ shows a conductivity of $2 \times 10^{-2} \text{ S cm}^{-1}$ at 800 °C [7], which is comparable to that of YSZ ($3.6 \times 10^{-2} \text{ S cm}^{-1}$ at 800 °C). CaMoO_4 is a representative scheelite compound, and its central Mo metal ion is coordinated by four O^{2-} ions in tetrahedral symmetry [8]. It can be easily doped with rare-earth ions, and the doped crystal can be used as an important function material. Recently, calcium molybdate based

mixed oxides have been of practical interest because of their attractive luminescence property and possibility of negative electrode (anode) materials [9,10]. More attention is focused on a lot of properties such as electrical properties, thermal properties, luminescence and reflectivity [11–14], which provide a basis for our understanding of this kind of material. Presently, possible applications of these materials in solid-state devices as electrodes and electrolytes have been studied by more and more researchers.

Various techniques have been developed to synthesize CaMoO_4 fine powders, such as molten salt, microwave irradiation, coprecipitation, sonochemical method and conventional solid-state reaction [15–18]. Sol–gel auto-combustion method has been studied in different ceramic systems recently; it combines the virtues of the sol–gel process and low temperature combustion process. This method has the advantages of inexpensive precursors and resulting nano-sized, homogeneous, highly reactive powders. Using this method, a single-phase powder can be formed at low temperature and the properties of the product can be improved.

In this paper, the $\text{Ca}_{1-x}\text{Sm}_x\text{MoO}_{4+\delta}$ powders were prepared using sol–gel auto-combustion process; the phase information and sinterability were investigated. Furthermore, the electrical properties were characterized to estimate if it could serve as an alternative electrolyte for SOFCs.

2. Experimental

Powder samples with the general formula of $\text{Ca}_{1-x}\text{Sm}_x\text{MoO}_{4+\delta}$ ($x = 0-0.3$) were synthesized by the sol–gel auto-combustion process. To synthesize nanocrystalline $\text{Ca}_{1-x}\text{Sm}_x\text{MoO}_{4+\delta}$,

* Corresponding author. Tel.: +86 551 2158437; fax: +86 551 2158437.

E-mail address: cjh@hfuu.edu.cn (J. Cheng).

analytical pure $\text{Sm}(\text{NO}_3)_3$, $\text{Ca}(\text{NO}_3)_2$, MoO_3 (AR grade, Sinopharm Chemical Reagent Co. Ltd., China) were used as starting materials. $\text{Sm}(\text{NO}_3)_3$ and $\text{Ca}(\text{NO}_3)_2$ were dissolved into deionized water, MoO_3 was dissolved into ammonia solution, then the two liquids were mixed together under continuous stirring at 80°C . Citric acid was then added as both a chelating and a reducing agent (the citric acid/metal molar ratio was fixed at 1.5), the pH value of the final solution was adjusted by $\text{NH}_3\cdot\text{H}_2\text{O}$. This mixed solution was then heated under stirring at 80°C to form a homogeneous sol, the sol was further heated at 80°C to get the gel, and then the gel was kept in an oven at 120°C for 24 h to get dried gel. The dried gel was calcined in an oven at $500\text{--}700^\circ\text{C}$, where the auto-combustion reaction took place to form the precursors. The powders were prepared by calcining the precursors at 900°C for 3 h. The obtained powders were pressed into pellets under 200 MPa. The pellets were heated to $1100\text{--}1300^\circ\text{C}$ in air at a heating rate of $1^\circ\text{C}/\text{min}$ and sintered for 4 h at different temperatures, then cooling down to room temperature naturally (furnace: KXS₂-6-16 energy conservation type fast elevation of temperature electric stove, Xiangtan Xiangyi instrument Co. Ltd., China).

Phase formation of the calcined oxide powders was determined by X-ray diffraction (XRD: Model D/max- γ B, Rigaku, Japan) analysis at room temperature with a Bragg angle range of $10\text{--}80^\circ$. Relative density of the sintered pellets was measured using the Archimedes' method, and the cross-sectional views of the samples were observed by scanning electron microscope with 5 kV and 5 mA (SEM: Model JSM-6400, JEOL, Japan). Electrical conductivity of the electrolyte materials was measured on the sintered pellet samples. Silver paste was used as electrodes painted on both sides of each pellet. The measurement of AC impedance was performed in air with an electrochemical workstation CHI660B (Shanghai Chen Hua Instrument Co. Ltd., China) in the frequency range 0.1 Hz to 100 kHz. The measurement curves were conducted in the temperature range $500\text{--}800^\circ\text{C}$ with an interval of 50°C . The conductivity at each temperature was obtained after stabilizing the specimens for 30 min.

3. Results and discussion

The XRD patterns of the $\text{Ca}_{1-x}\text{Sm}_x\text{MoO}_{4+\delta}$ powders calcined at 900°C for 3 h are shown in Fig. 1. All diffraction peaks match well with JCPDS file No. 08-0144. No additional diffraction peaks were found, indicating the substitution of Sm^{3+} ion to Ca^{2+} site has taken place. The Sm^{3+} ions dissolved in the crystal lattice of CaMoO_4 completely, and formed a solid solution with single tetragonal scheelite phase.

The tetragonal scheelite-type $\text{Ca}_{1-x}\text{Sm}_x\text{MoO}_{4+\delta}$ solid solution is to extend up to $x = 0.3$ in this system, which is comparable to that in the previous reports [19]. In this composition range, a shift in the peak position is not obvious, but, the lattice parameters of the tetragonal phase changed and the anion lattice distorted with samarium content due to the size differences between Sm^{3+} and Ca^{2+} . Table 1 lists the lattice parameters of $\text{Ca}_{1-x}\text{Sm}_x\text{MoO}_{4+\delta}$ samples (the lattice parameters were determined by Rietveld refinement). As can be seen from Table 1, the lattice parameters

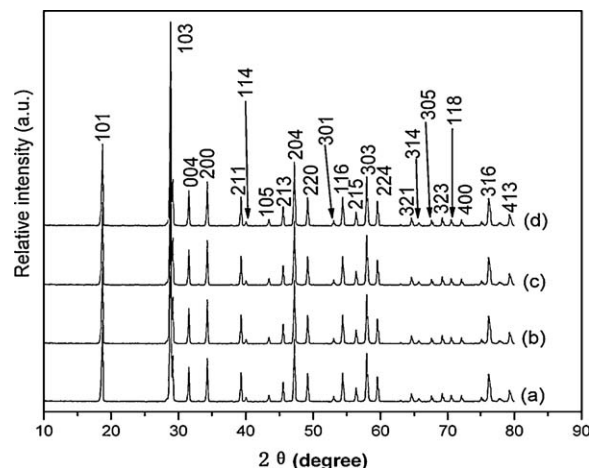


Fig. 1. X-ray diffraction patterns of $\text{Ca}_{1-x}\text{Sm}_x\text{MoO}_{4+\delta}$ samples: (a) $x = 0$, (b) $x = 0.1$, (c) $x = 0.2$, and (d) $x = 0.3$.

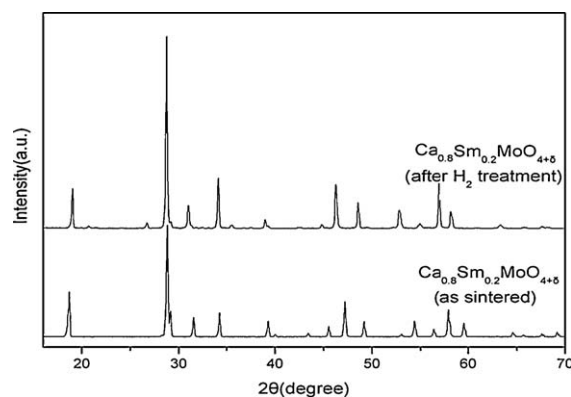


Fig. 2. X-ray diffraction pattern of $\text{Ca}_{0.8}\text{Sm}_{0.2}\text{MoO}_{4+\delta}$ before and after exposing to H_2 atmosphere at 900°C for 2 h.

increased with increasing x in the Sm-substituted system. Furthermore, the volumes of the unit cells increase with increasing x , could be understood by considering the substitution for Ca^{2+} by the trivalent Sm^{3+} cation having bigger ionic radius. As we know, the radii of Ca^{2+} and Sm^{3+} are 0.099, 0.108 nm, respectively [20,21], when doped with larger sized Sm^{3+} ions, the tetragonal CaMoO_4 lattice will expand.

In order to verify the stability in a reducing atmosphere, the sintered samples were exposed to H_2 atmosphere at 900°C for 2 h and phase composition of the resulting specimens was investigated. Fig. 2 shows the X-ray diffraction patterns of the surface of the sintered $\text{Ca}_{1-x}\text{Sm}_x\text{MoO}_{4+\delta}$ before and after exposing. The diffraction pattern of the specimen after H_2 treatment was same as that of before untreated sample. That is to say, Scheelite-type $\text{Ca}_{1-x}\text{Sm}_x\text{MoO}_{4+\delta}$ materials have high chemical stability under reducing atmospheres, and meet the requirement of the electrolyte in SOFCs.

Table 1

x Value	Lattice constant (nm)		The unit cells' volume (nm^3)	Theoretical density (g cm^{-3})	Sintered density (g cm^{-3})
	a	c			
$x = 0$	0.5226	1.1439	0.3121 ^a	4.259 ^a	
$x = 0.1$	0.5345	1.1649	0.3319	4.471	4.327
$x = 0.2$	0.5454	1.1738	0.3491	4.683	4.518
$x = 0.3$	0.5561	1.1959	0.3694	4.893	4.713

^a Unit cell volume and theoretical density evaluated from the tetragonal scheelite-type structure of CaMoO_4 (JCPDS file No. 08-0144).

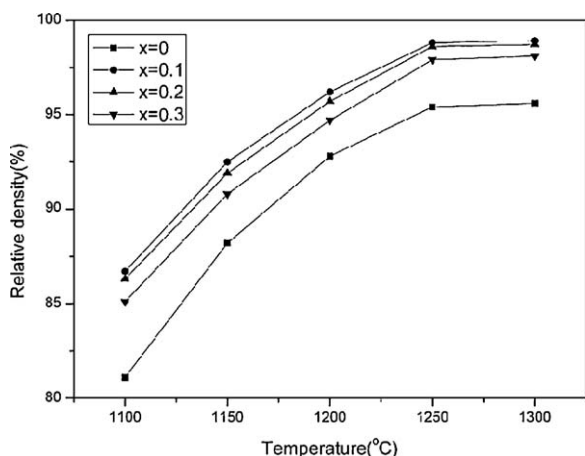


Fig. 3. Dependence of relative density on sintering temperatures for $\text{Ca}_{1-x}\text{Sm}_x\text{MoO}_{4+\delta}$ ceramics.

Relative density of the sintered pellets was measured using the Archimedes' method. Fig. 3 shows the relative density of $\text{Ca}_{1-x}\text{Sm}_x\text{MoO}_{4+\delta}$ ceramics sintered at different temperatures. The density of sintered $\text{Sm}_x\text{Ca}_{1-x}\text{MoO}_{4+\delta}$ ceramics increases as temperature is increasing, and a maximum relative density (98.7%) of the theoretical was obtained at a sintering temperature of 1250 °C, which satisfied the requirement for SOFCs electrolytes operating at intermediate temperature. When sintering temperature is over 1250 °C, the density of sintered ceramics can hardly improve, so the ideal sintering temperature of $\text{Ca}_{1-x}\text{Sm}_x\text{MoO}_{4+\delta}$ ceramics is 1250 °C. On the other hand, the relative density of $\text{Ca}_{1-x}\text{Sm}_x\text{MoO}_{4+\delta}$ sintered ceramics decrease on a small scale with increasing x , it could be understood by considering the substitution of the difference of cation sizes.

Fig. 4 shows the cross-sectional views of $\text{Ca}_{0.8}\text{Sm}_{0.2}\text{MoO}_{4+\delta}$ electrolyte sintered under 1150 °C and 1250 °C for 4 h. There exists a small quantity of pores in the sintered pellet at 1150 °C (Fig. 4a). The sintered electrolyte pellet sintered at 1250 °C (Fig. 4b) is quite dense and uniform, the cross-sectional view without any obvious

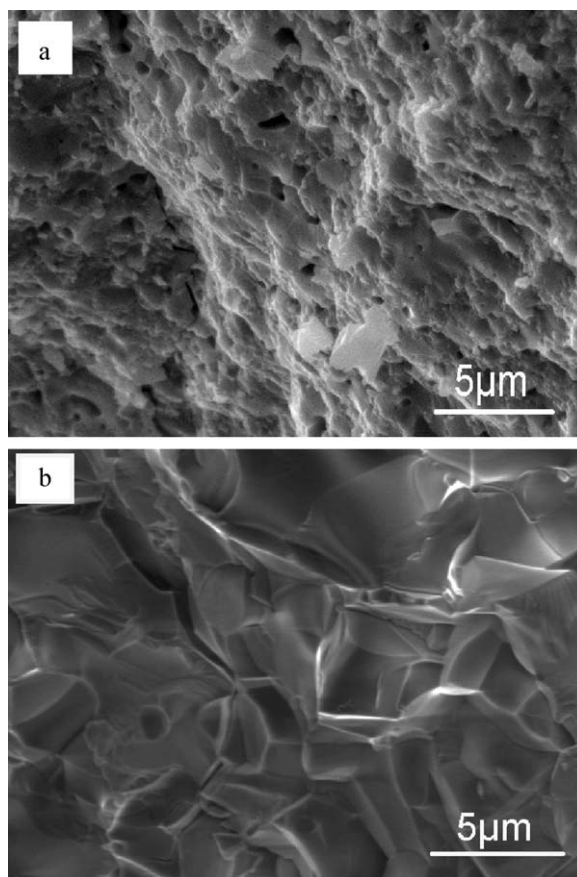


Fig. 4. Cross-section of $\text{Ca}_{0.8}\text{Sm}_{0.2}\text{MoO}_{4+\delta}$ electrolyte: (a) 1150 °C and (b) 1250 °C.

pores and cracks indicating good sintering. Therefore, we selected the pellets sintered at 1250 °C as the objects of study in this paper.

Fig. 5 shows typical impedance plots for $\text{Ca}_{0.8}\text{Sm}_{0.2}\text{MoO}_{4+\delta}$ pellets sintered at 1250 °C for 4 h measured in air at various temperatures. Impedance spectra at high temperatures (Fig. 5b–d)

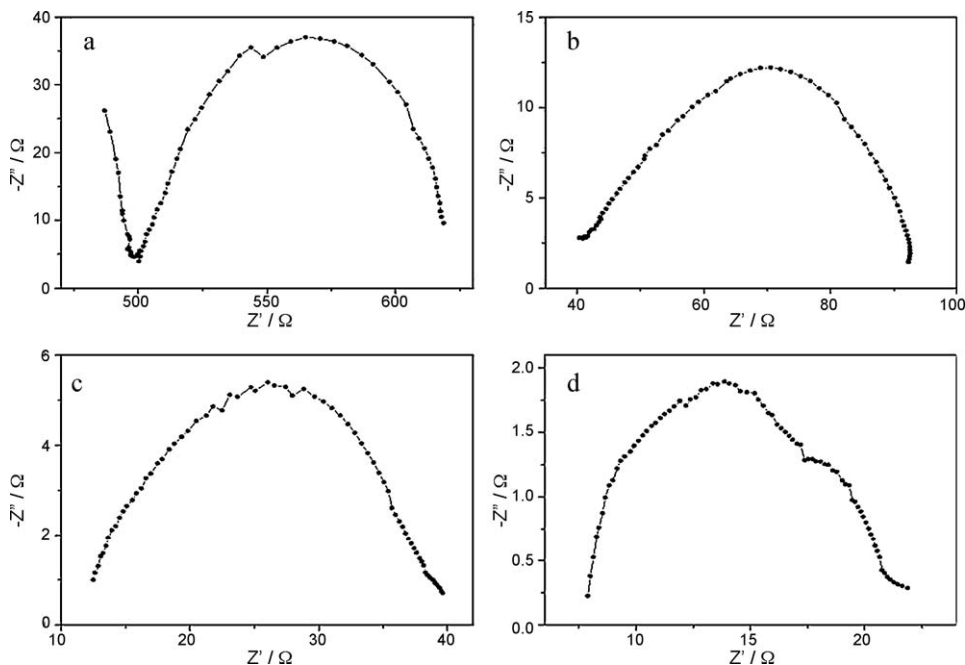


Fig. 5. Impedance spectra of $\text{Ca}_{0.8}\text{Sm}_{0.2}\text{MoO}_{4+\delta}$ tested at: (a) 500 °C, (b) 600 °C, (c) 700 °C, and (d) 800 °C.

Table 2

t ($^{\circ}\text{C}$)	500	550	600	650	700	750	800
R (Ω)	497.6	147.2	40.9	19.1	12.5	9.2	7.9
σ (S cm^{-1})	1.51×10^{-4}	5.12×10^{-4}	1.84×10^{-3}	3.94×10^{-3}	6.03×10^{-3}	8.19×10^{-3}	9.54×10^{-3}

show one dominating semicircle, as well as a non-zero axis intercept on the high frequency side. At lower temperatures (Fig. 5a), an additional arc at intermediate frequencies becomes clearly visible. The resistances associated with these three processes are referred to as R_b , R_i and R_s , respectively. The impedance spectra data were fitted with suitable equivalent circuit of the Zview software to distinguish the bulk resistance and grain-boundary resistance, and the conductivities were calculated. The total resistance of electrolyte can be obtained from the spectra and converted to a conductivity datum σ , using the relation:

$$\sigma = \frac{L}{RS} \quad (1)$$

where L is the sample thickness and S is the electrode area on the sample surface, and these parameters are compiled in Table 2. With the increase of the operating temperature, the total resistance decreases, and the electrical conductivity datum increases. The conductivity of $\text{Ca}_{0.8}\text{Sm}_{0.2}\text{MoO}_{4+\delta}$ sintered at 1250°C for 4 h in air reached $9.54 \times 10^{-3} \text{ S cm}^{-1}$ under the testing temperature of 800°C . This value is close to that of other electrolytes working in intermediate temperature range [20,22], indicating that samarium doped CaMoO_4 is a promising electrolyte for intermediate-temperature SOFCs.

Representative Arrhenius plots of conductivity measured in air are shown in Fig. 6. It is remarkable to see that enhanced conductivities are observed in the samples substituted by samarium (for pure CaMoO_4 , the conductivity is $5.0 \times 10^{-5} \text{ S cm}^{-1}$ at 800°C [23]), it increased gradually with increasing samarium content within the solubility range. Nevertheless, when the samarium content exceeded 20%, the conductivity decreased. In the temperature range of the measurements, the highest conductivity is observed in the $x = 0.2$ sample.

The Arrhenius plot is on a logarithmic scale and the activation energies for $\text{Ca}_{1-x}\text{Sm}_x\text{MoO}_{4+\delta}$ samples can be obtained from Arrhenius plots in Fig. 6. In the case that the conductivities show small breaks at $600\text{--}650^{\circ}\text{C}$, they were calculated in two temperature regions, above 650°C and below 600°C . These temperatures demarcate the two conductivities contribution by the two different types of charge carriers [23].

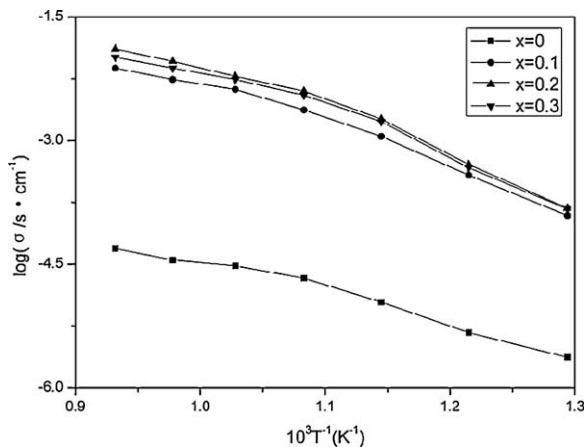


Fig. 6. Arrhenius plot comparing the total electric conductivity of $\text{Ca}_{1-x}\text{Sm}_x\text{MoO}_{4+\delta}$.

The conductivity at the high temperature region ($>650^{\circ}\text{C}$) is expressed by

$$\sigma T = A_1 \exp\left(-\frac{E_1}{\kappa T}\right) \quad (2)$$

with

$$E_1 = \frac{1}{2} h_f + h_m \quad (3)$$

where h_f is the energy of formation of Frenkel defects and h_m is the migration energy of the mobile species. At low temperature ($<600^{\circ}\text{C}$), the conductivity being determined by the frozen-in defects, is given by

$$\sigma T = A_2 \exp\left(-\frac{E_2}{\kappa T}\right) \quad (4)$$

where

$$E_2 = h_m \quad (5)$$

Should the same carrier be mobile in the two temperature regions, the Frenkel defect formation energy h_f can be computed from Eqs. (3) and (5) as

$$h_f = 2(E_1 - E_2) \quad (6)$$

The activation energies E_1 and E_2 , calculated from the two slopes are presented along with Frenkel defect formation energy of each of the different crystal compositions. It is essentially implied that the activation enthalpy of the low temperature region is lower than the one of the high temperature conductivity [19,23]. The activation energies for $\text{Ca}_{0.8}\text{Sm}_{0.2}\text{MoO}_{4+\delta}$ sample in the two temperature regions are 0.55 eV and 0.85 eV, respectively.

In order to check the charge carriers in $\text{Ca}_{1-x}\text{Sm}_x\text{MoO}_{4+\delta}$, the following oxygen gas concentration cells were constructed using sample pellets as electrolytes, and the cell EMFs were measured:



Fig. 7 shows EMFs measured by oxygen gas concentration cells constructed using samples as the electrolytes, air and 1 atm oxygen gas as the anode and cathode gas, respectively. Measured EMFs for $\text{Ca}_{1-x}\text{Sm}_x\text{MoO}_{4+\delta}$ showed good coincidence with the

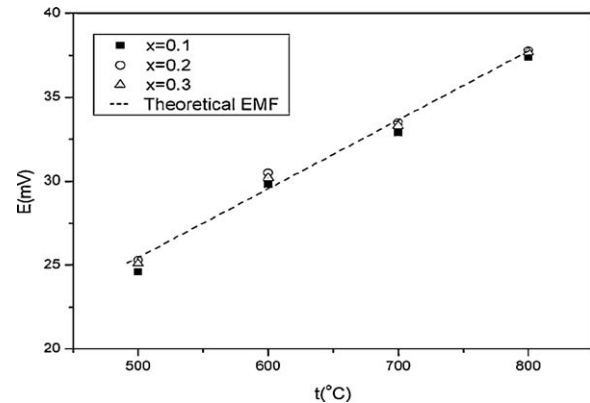


Fig. 7. Temperature dependence of the EMF of the cell: O_2 (0.21 atm), $\text{Ag}[\text{Ca}_{1-x}\text{Sm}_x\text{MoO}_{4+\delta}]\text{Ag}$, O_2 (1 atm). The dashed line denotes the theoretical EMF obtained by the Nernst equation.

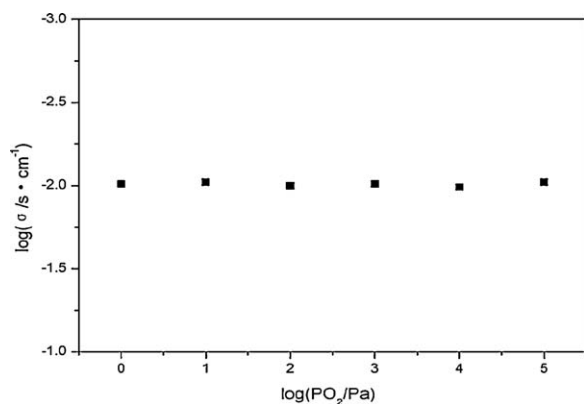


Fig. 8. Electrical conductivity of $\text{Ca}_{0.8}\text{Sm}_{0.2}\text{MoO}_{4+\delta}$ at 800 °C as a function of oxygen partial pressure.

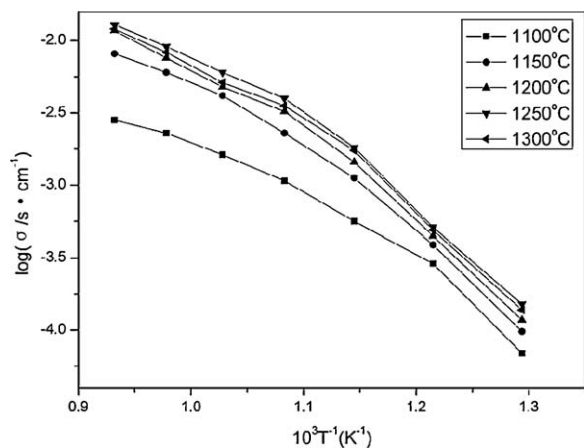


Fig. 9. Dependence of the conductivity on temperature for $\text{Ca}_{0.8}\text{Sm}_{0.2}\text{MoO}_{4+\delta}$ ceramic.

value of the theoretical EMF for oxygen concentration cell calculated (E) from the Nernst equation, indicating that the ionic transport number of this compound was almost unity. In Fig. 8, electrical conductivities of $\text{Ca}_{0.8}\text{Sm}_{0.2}\text{MoO}_{4+\delta}$ are shown as a function of oxygen partial pressure. For the oxygen partial pressure measurements, we used the method which has been reported by Norby and Kofstad [24]. Controlled oxygen partial pressures were established by mixing air with deoxidized argon, by means of calibrated flowmeters. The mixing stage was initially checked with a zirconia oxygen probe, but no monitor was used for the oxygen activity in the cell during the measurements. As seen in Fig. 8, the conductivity does not change with oxygen partial pressure, which indicated that the electron and vacancy do not contribute to the conductivity. These results indicate that the main ionic charge carriers were oxide ions.

In order to investigate the effect of sintering temperature on the properties of $\text{Ca}_{1-x}\text{Sm}_x\text{MoO}_{4+\delta}$, a series of sintering conditions

were studied. Fig. 9 shows the logarithm of electrical conductivity versus reciprocal temperature of $\text{Ca}_{0.8}\text{Sm}_{0.2}\text{MoO}_{4+\delta}$ samples sintered for 4 h at different temperatures and then measured at 800 °C in air. As seen from Fig. 9, the electrical conductivity datum increases with the increase of the sintering temperature, and reaches an ideal value at 1250 °C. However, when the sintering temperature exceeded 1250 °C, the conductivity decreased. The reason may be that the lattice oxygen loss of this system at high temperatures caused the decrease of electrical conductivity due to the reduction of charge carrier concentration [25].

4. Conclusions

The sol-gel auto-combustion process was used to synthesize scheelite-type electrolyte materials, $\text{Ca}_{1-x}\text{Sm}_x\text{MoO}_{4+\delta}$ ($x = 0-0.3$). Their phase formation, sintering behaviors and electrochemical properties were investigated. The result shows, when doped with larger Sm^{3+} ions, the scheelite lattice of CaMoO_4 will expand. $\text{Ca}_{1-x}\text{Sm}_x\text{MoO}_{4+\delta}$ samples show higher sinterability than pure CaMoO_4 , and the $\text{Ca}_{1-x}\text{Sm}_x\text{MoO}_{4+\delta}$ sample with 98.7% of the theoretical density can be obtained after being sintered at 1250 °C for 4 h. The total conductivity peaks at $x = 0.2$ in the temperature range of 500–800 °C for Sm-doped CaMoO_4 electrolyte materials.

Acknowledgement

This work was kindly supported by the Natural Science Foundation of Education, Department of Anhui province under contract No. KJ2009B045Z.

References

- [1] Y.C. Liou, S.L. Yang, J. Power Sources 179 (2008) 553.
- [2] F. Baratto, U.M. Diwekar, J. Power Sources 139 (2005) 188.
- [3] J.S. Ahn, D. Pergolesi, M.A. Camaratta, H. Yoon, B.W. Lee, K.T. Lee, D.W. Jung, E. Traversa, E.D. Wachsman, Electrochem. Commun. 11 (2009) 1504.
- [4] C. Feng, H. Li, P. Zhang, Z. Guo, H. Liu, Mater. Chem. Phys. 119 (2010) 82.
- [5] Y. Matsuzaki, Y. Baba, T. Sakurai, Solid State Ionics 174 (2004) 81.
- [6] R. Hansch, M.R.R. Chowdhury, N.H. Menzler, Ceram. Int. 35 (2009) 803.
- [7] T. Esaka, Solid State Ionics 136–137 (2000) 1.
- [8] X. Li, Z. Yang, L. Guan, J. Guo, Y. Wang, Q. Guo, J. Alloys Compd. 478 (2009) 684.
- [9] A. Selmi, G. Corbel, P. Lacorre, Solid State Ionics 177 (2006) 3051.
- [10] P. Pinet, J. Fouletier, S. Georges, Mater. Res. Bull. 42 (2007) 935.
- [11] A. Phuruangrat, T. Thongtem, S. Thongtem, J. Alloys Compd. 481 (2009) 568.
- [12] C.H. Cui, J. Bi, D.J. Gao, Mater. Lett. 62 (2008) 2222.
- [13] T.Y. Liu, J. Chen, F.N. Yan, J. Lumin. 129 (2009) 101.
- [14] N. Sharma, K.M. Shaju, G.V. Subba Rao, B.V.R. Chowdari, Z.L. Dong, T.J. White, Chem. Mater. 16 (2004) 504.
- [15] Y. Wang, J. Ma, J. Tao, X. Zhu, J. Zhou, Z. Zhao, L. Xie, H. Tian, Ceram. Int. 33 (2007) 693.
- [16] F. Lei, B. Yan, J. Solid State Chem. 181 (2008) 855.
- [17] V. Thangadurai, C. Knittlmayer, W. Weppner, Mater. Sci. Eng. B 106 (2004) 228.
- [18] T. Thongtem, A. Phuruangrat, S. Thongtem, J. Ceram. Process. Res. 9 (2008) 189.
- [19] T. Esaka, R. Tachibana, S. Takai, Solid State Ionics 92 (1996) 129.
- [20] S.W. Zha, C.R. Xia, G.Y. Meng, J. Power Sources 115 (2003) 44.
- [21] R.D. Shannon, Acta Crystallogr. A 32 (1976) 751.
- [22] D. Lee, J.H. Han, Y. Chun, R.H. Song, D.R. Shin, J. Power Sources 166 (2007) 35.
- [23] S.K. Arora, R.S. Godbole, D. Lakshminarayana, J. Mater. Sci. 18 (1983) 1359.
- [24] T. Norby, P. Kofstad, J. Am. Ceram. Soc. 69 (1986) 784.
- [25] H. Zhao, D. Teng, X. Zhang, C. Zhang, X. Li, J. Power Sources 186 (2009) 305.